A MECHANISTIC ASSESSMENT OF STRUCTURAL FAILURE FOR MISSILE IMPACTS ON CONCRETE STRUCTURES

P. GODBOUT, A. BRAIS

Nuclear Engineering Institute, Université de Montréal,
Case Postale 6079, Montréal, Québec H3C 3A7, Canada

The need for a thorough unified analytical study encompassing all phenomenological and behavioral phases of both projectile and structure under failure coupled with a well documented experimental test data bank is evident to allow extrapolation with much greater confidence beyond the range of the available data. This study was done for the Atomic Energy Control Board of Canada. While our analytical modeling and simulations addressed themselves principally to CANDU Reactor Type outer-containment and to projectiles having low velocities (20-200 m/sec), large diameters (20-140 cm) and large masses (65-3,000 kg) the methodology used can also be used for the study of high velocity (in excess of 300 m/sec), small mass and small diameter (less than 40 cm) projectiles including blast waves. A new methodology is developed for the analysis of the structural behavior of reactor outer-containment structures subject to projectile impacts. A unified physical model is established that comprises both missile and target material constitutive equations and permits the impact phenomena to be simulated using an action-reaction technique rather than imposed forces or velocities. Such an approach renders the model under study independent of actual system parameters and therefore allows unrestricted scaling, and is applicable to both hard and soft projectiles. Materials behavior under all phases of physical stresses and strains including physical state changes for the system under study are well enough known and understood to allow the setting up of reliable constitutive equations in our analytical models. This mechanistic formulation is amenable to simulating using finite-difference techniques. Numerical simulations have been performed using the PISCES-2DELK system of codes which allows the interaction of a number of grids together, taking advantage of a coupled Euler-Lagrange formulation. A parallel in-depth study of stress wave phenomena was performed which has enabled us to identify phenomenalogically distinct phases within the overall impact process. This allows an overall simulating procedure which is segmented in time and comprises of both numerical and purely analytical phases and thus savings in computer costs which are considerable. The model is validated using experimental test data from France either obtained from open literature or obtained by direct negociations with the organizations of concern (EDF and CEA). Numerical results agree well with the available data. Calculations show that backface reinforcement is a key design aspect in preventing perforation and plug ejection as the stretching and striction of the re-bar grid can absorb a considerable fraction of the missile kinetic energy. Calculations clearly and properly identify all phases and physical aspects of plug formation and, when applicable, ejection. Calculations show that a hard projectile cannot be considered rigid except for the purpose of obtaining upper bounds for perforation and penetration, an upper bound for plug size formation and physical characteristics, upper bound for plug ejection velocities, etc. Numerical results agree well for all phenomenalogical phases and physical results with the available experimental data which include cinematographical records of impact tests. The final result of this study is a handbook-type tool in a format which seeks implementability optimization for both design and safety related analyses.

1. Introduction

In recent years, a number of formulae have been developed to describe impactive penetration processes, such as the Petry, BRL, Army Corps of Engineers and NDRC formulae. Detailed information about the latter formulae or authors may be found in a paper by Kennedy |1|.

All of the above empirical relations are based on experiments conducted using high velocity (in excess of 300 m/s), low mass and small diameter (below 40 cm) projectiles, and are valid only within the range of variables for which experimental data is available.

Renewed interest in this field of study has recently been shown by nuclear regulatory agencies, concerned with finding a sound design basis for nuclear reactor containment structures. The range of variables encountered in the problem of external hazards to nuclear power plants (in particular the case of aircraft-generated hard projectile impacts) is, in general, very different, since we are concerned here with projectiles of low-velocity (2-200 m/s), large diameter (20-140 cm) and large mass (65-3,000 kg), which are not within the range of applicability of the above and other available empirical formulae.

Many experimental programs were initiated to overcome this gap, so that today additional information is available from tests conducted in the US, France, Germany, UK and Australia, pertaining either to tornado or aircraft crash generated missiles. Unfortunately, these tests span only a small portion of the possible aircraft impact situations.

There was a clear need for a comprehensive analytical study encompassing all phases of the penetration and perforation processes, together with verification by experimental data and computer simulations, in order to gain a better understanding and allow extrapolation with much greater confidence beyond the range of the available data and formulae.

This paper presents such an approach towards the formulation of successive impact processes such as shock wave, flow-type penetration and reinforcement-grid stretching in impact of hard projectiles on reinforced-concrete walls of the type found in our Canadian CANDU nuclear reactor containment structures.

A previous phase of this study |2| addressed itself to the description and characterization of aircraft crash-related projectiles which might be expected in the vicinity of large-scale airports. Accordingly, over 150 types of both heavy and light aircraft currently in use in Canada were classified into 43 precisely defined projectile categories. The coupling of the analytical model with the missile parameters resulted in different load impact characteristics for each category, an approach which necessarily involved much time, effort and simulation costs for analysis.

There was a clear need for a thorough analytical study, the results of which would be useful in bringing together all the necessary tools, techniques, graphs, tables, etc. in handbook format, within the guidelines of being sufficiently specific on the results sought and minimizing analytical costs, a need which had been clearly expressed for some time by our Nuclear Regulatory Commission.

A study approach was proposed and accepted which involved analyses, experiments and computer simulations to identify the phenomenologically different key phases in the processes involved. This has enabled us to use a segmented approach to evaluation, so that efforts and precision needed in simulation may be minimized for any future analytical design requirements.

Our results show clearly that precise, detailed simulations are needed only for the initial phase of the impact process, while the remaining processes may confidently be evaluated using a rough simulation approach, much less specialized computer programs, and in many cases manual calculations only, based on data contained in properly designed tables, graphs or similar tools or techniques.

The above results apply to hard projectile impacts on reinforced concrete structures of the CANDU type.

2. Experimental Data

In verifying our analytical model, materials, constitutive equations and associated computer code simulator, we simulated missile-target systems and cases representative of actual experiments done in the US, France, Germany, UK and Australia, and for which adequate experimental data was readily available.

One such simulation used as an example consisted of a scaled-down impact on a reinforced concrete slab, such as had been done by Electricité de France jointly with the Commissariat à l'Energie Atomique [3].

The experimental apparatus consisted of a cylindrical, flat-nosed steel projectile with a mass of 227 kg, a diameter of 30.5 cm and an impact speed of 126.8 m/sec.

The target consisted of a square reinforced concrete slab, 50 cm thick and 500 cm wide. The reinforcement, similar to that used in CANDU structures, consisted of two rebar layers, one near the front face, the other near the back face. The available data for this experiment consisted of penetration versus time curves as obtained from filmed records, as well as slab sections showing cratering and rebar position after impact (Fig. 1).

3. Analytical Models

The french experiment was simulated using the PISCES 2DELK computer code [6]. PISCES is a two-dimensional, time-dependent and finite-difference code which allows the interaction of a number of grids together, taking advantage of a coupled Euler-Lagrange formulation.

The differential equations which govern material motion are applied to a network of zones or a grid which describes the geometry of the problem.

In this problem, the steel projectile was modeled as a Lagrange grid (deformable). The target was modeled using a Lagrange grid with an encased Euler grid in the vicinity of the impact area as shown in Figure 2.

While the Lagrange grid deforms, the Euler grid is fixed in space and allows mass transfer from zone to zone. This is advantageous for the concrete impact area where velocities and deformations are considerable.

The use of an Euler grid prevents costly time-step degrading and inconvenient rezonings while, on the other hand, the Lagrange grid allows the material history of concrete to be preserved.

Basically, the mathematical model used in simulating comprises a set of coupled equations which gives, locally, a complete description of the motion of a continuum and, therefore, of the dynamics of behavior for that zone. It takes into account the laws of conservation of mass, momentum and energy including both the initial and boundary conditions and a material model relating stress to deformation.

For the mathematical considerations to follow, we will be using the Lagrangian system of coordinates and a two-dimensional axisymmetrical formulation. The axis of symetry is

represented by X, the time derivatives by dots and the direction perpendicular to the X-Y plane by Z. Conservation of mass is implicitely satisfied in Lagrange coordinates such that the volume V of this mass and at all times is obtained from the geometry of deformation. The density term is therefore given by

$$\rho = \rho o \; Vo/V \tag{1}$$

Conservation of momentum and the material model are coupled using a stress tensor T as follows :

$$\rho\ddot{x} = \frac{\partial}{\partial x} T_{xx} + \frac{\partial}{\partial y} T_{xy} + T_{yy}/y \tag{2}$$

$$\rho\ddot{y} = \frac{\partial}{\partial x} T_{xy} + \frac{\partial}{\partial y} T_{yy} + (T_{yy} - T_{zz})/y \tag{3}$$

The stress tensor is further broken down into a spherical term corresponding to the hydrostatic pressure P and into a deviatoric term S as follows :

$$T_{xx} = -P + s_{xx} \tag{4}$$

$$T_{yy} = -P + s_{yy} \tag{5}$$

$$T_{zz} = -P + s_{zz} \tag{6}$$

$$T_{xy} = s_{xy} \tag{7}$$

The spherical term accounts for the volumetric change while the deviatoric term is descriptive of the resistance of the material to shear distortion. The elastic changes in the stress deviators are expressed as follows :

$$s_{xx} = 2G \left(\dot{\varepsilon}_{xx} - \frac{1}{3} \cdot \frac{\dot{V}}{V}\right) \tag{8}$$

$$s_{yy} = 2G \left(\dot{\varepsilon}_{yy} - \frac{1}{3} \cdot \frac{\dot{V}}{V}\right) \tag{9}$$

$$s_{zz} = 2G \left(\dot{\varepsilon}_{zz} - \frac{1}{3} \cdot \frac{\dot{V}}{V}\right) \tag{10}$$

$$s_{xy} = 2G \; \dot{\varepsilon}_{xy} \tag{11}$$

where G represents the shear modulus which is assumed constant. The deviators are further adjusted for material rotation, spall and plasticity. The yield model can be visualised as a function which controls the stress deviators with regard to plasticity : it represents a relation between a value Y and the hydrostatic pressure P prevailing for a given state of stress. For every stress state, the Von Mises yield stress which is directly related to the second invariant of the stress deviator is calculated and then compared with the computed value of Y. If the calculated yield stress exceeds Y, the material is yielding and the deviators are corrected in order to conserve the value Y. The yield model is formulated in such a way as to allow recall of the past stress history of the concrete.

The strain rates are related to the local velocity $\vec{v} = (x, y)$ as follows :

$$\dot{\varepsilon}_{xx} = \partial\dot{x}/\partial x \tag{12}$$

$$\dot{\varepsilon}_{yy} = \partial\dot{y}/\partial y \tag{13}$$

$$\dot{\varepsilon}_{xy} = 1/2 \; (\partial\dot{x}/\partial y + \partial\dot{y}/\partial x) \tag{14}$$

$$\dot{\varepsilon}_{zz} = \dot{y}/y \tag{15}$$

The relative volumetric rate of change at a point in the material is related to the strain rates as follows :

$$\dot{V}/V = \dot{\varepsilon}_{xx} + \dot{\varepsilon}_{yy} + \dot{\varepsilon}_{zz} \qquad (16)$$

The model used in setting up the equation of state is descriptive of the hydrostatic pressure P as a function of the change in relative density $\mu = (\rho - \rho o)/\rho$ and of the external energy e.

$$P = f(\mu, e) \qquad (17)$$

The equation of energy conservation is as follows :

$$e = \frac{1}{s}\left(T_{xx}\,\dot{\varepsilon}_{xx} + T_{yy}\,\dot{\varepsilon}_{yy} + T_{zz}\,\dot{\varepsilon}_{zz} + 2T_{xy}\,\dot{\varepsilon}_{xy}\right) \qquad (18)$$

Equations (17) and (18) must be solved simultaneously.

Since the setting up of the Euler system of equation is analogous, it will not be covered in this paper.

4. Assumptions

It is assumed, for both the steel and concrete models, that the hydrostatic pressure is a function of material density alone : while impact processes do generate heat it does not represent, in our cases, a significant portion of the total kinetic energy used.

Steel was modeled as a linear-elastic and perfectly plastic material. Most steel parameters used were from a report on blunt projectile impact simulations done by Physics International |4|.

The equations of state used for concrete are adapted forms of the ones used by ATTALA and NOWOTNY |5|. The numerical data used were also adapted to suit our specific needs and were obtained from hydrostatic loading tests data results |7|.

The specific and particular construction characteristics of a CANDU reinforced containment wall has enabled us, in simulating, to separate the late influence of reinforcement grids from that of the early impact effects on concrete. This allowed us to use a concrete material model alone and without the need also include, in simulating, that of a reinforcement model.

If a concrete sample is hydrostatically compressed (Fig. 3), the relative density change μ increases along the line OA. The slope of this line is the bulk modulus K. Loadings beyond A will cause the concrete to collapse and in such a way that the grains are reordered in a more compacted form as the volume of the pores decreases. Point A is defined as the collapse hydrostatic pressure or Pcoll; its value is three to five times the single axial compressive strength. When the volume further decreases, the pressure moves to the right on line AC with a decreased slope and until complete compaction occurs at C where the slope becomes again K.

Further refinements to the model include such things or void opening when a load release occurs along the line AC and loss of tensile strength whenever load release occurs after a collapse or yield or tensile failure. Abrupt slope transitions were also eliminated in order to improve the numerical response of the model.

Exploratory computer simulations have shown that structural inertial effects resulting from a high-energy hard projectile are far too high to allow the structure to respond globally to such an impact before the advent of essentially local damage such as penetration and perforation.

Some simulations were carried out using a rigid model for the projectile. The results show that the pressures generated ahead of the projectile were about 50% higher than those calculated using a deformable steel model, and therefore accentuated the true level of damage.

5. Impact Processes and Analyses

The analytical study of impact processes must take into account the properties of stress waves which, for flat-nosed missiles, are relatively simple to describe.

A stress wave is a transient stress disturbance which travels at a finite velocity from the area of application of the load. Two vectors are generated. The first is the longitudinal or dilatational wave which is indicative of particle motion parallel to the direction of propagation of the impulse while the strain is pure dilatation. The second is the transverse or distortional wave which is indicative of particle motion perpendicular to the direction of propagation of the impulse, the strain being pure shear. Distortional waves are considerably slower than dilatational waves.

Proper representation of a pulse may be in terms of stress versus distance. Impact generated stress waves can be approximated as shown in Figure 4.

For any wave traveling in a material, the moment it reaches a free surface it is totally or partially reflected, depending on the angle of incidence.

For a dilatational wave, therefore, the reflected energy will vary depending on whether the wave reaches a free surface obliquely or perpendicularly. Reaching a free surface perpendicularly represents the simplest case where the reflected wave (pulse) is equal but opposite in sign to that of the incident wave; that is, compression is reflected as tension, and so on.

When a dilatational pulse strikes a surface, both a dilatational and a transverse wave are reflected. The angle of the reflected dilatational wave is equal to the angle of incidence α as shown in Figure 5. We now define the coefficient of reflection R as the ratio of the reflected dilatational stress to the incident dilatational stress. It can be shown that R may have a negative or a positive value depending on both the angle of incidence and Poisson's Ratio ν (for concrete, $\nu \simeq 0.19$) as shown in Figure 6. A positive value for R indicates that the reflected stress is actually compressive.

Because of wave superposition, whenever a reflected tensile pulse meets the remainder of the incident compressive pulse, the net stress can be tensile and may thus exceed the tensile strength of the material. This may result in multiple spalls, and the ensuing generation of small secondary projectiles from the back face. This is especially true of concrete which has been previously weakened and yielded by the incident compressive wave, either by crushing or by yielding, such that its tensile strength is very low.

The impact of a flat-nosed cylindrical missile results in a stress wave front which combines plane and cylindrical fronts (Fig. 7).

The plane wave front does not diverge, and the stress of the wave remains constant, except for material attenuation and wave shape changes.

The cylindircal wave front does however diverge so that the stresses at any two points are inversely proportional to the square roots of their respective distance from the source. The cylindrical wave therefore, weakens with distance; furthermore, the intensity of the reflected tensile wave decreases with respect to the incident angle until and upon reaching an angle $\alpha = 50^{\circ}$ (for concrete) it begins to reflect as a compressive wave (Figure 6).

As can be seen in Figure 8, a well defined and almost conical fracture zone appears. The latter phenomenon appears quite clearly in one of our simulations as shown in Figure 9; it represents a computer simulation of an actual french experiment for which the experimental results are graphically shown in Figure 1.

The diameter D_c of the backface crater can therefore be estimated from thoery and reads as follows :

$$D_c \simeq D + \frac{2T}{\text{tg } 40^o} = D + 2.38T \qquad (19)$$

where D is the projectile diameter and T the slab thickness. It should be noted that, within the range of interest for the variables D & T, our eq. (19) is within 15% of another related formulation which, on the other hand, has been empirically formulated from experimental data results [8].

The plane portion of the reflected wave travels until it reaches the projectile's nose. This is the end of the shock phase. During this phase, the average pressure against the projectile's nose is high and barely decreases as shown in Figure 9 and which represents computer simulation results for the experimental set up of Figure 1. In Figure 10 we have the simulated pressure contours ahead of the missile during the shock phase.

The sharp drop in the average pressure curve (Fig. 9) represents the arrival of the tensile reflected wave.

From that moment on, the material ahead of the projectile is being fractured and offers greatly decreased resistance. It is called a penetration phase and it can be phenomenologically compared to a nearly steady flow of material past the projectile's nose.

In this phase, unlike the shock phase, the projectile's deceleration is quite low and the missile's velocity remains almost constant.

The penetration phase continues until the grid stretching phase occurs that is, when the missile meets with the back face grid of reinforcing bars. The stretching of such a grid is presently being studied in detail in order to determine, within reasonable and confident bounds, the energy that can be absorbed in this process. The importance of rear reinforcement design is great since this is the last structural component to absorb some or all of the remaining missile's kinetic energy; on the other hand, it must be remembered that the shock phase, in this regard, is much more important.

The front layers contribute, in themselves, little in slowing down the missile; since the "net" effect is absent, the layers are virtually punched through and with little energy expended.

Since the projectile is modeled as a non-rigid object, large velocity (and strain) gradients are usually present along the length so that interpretation of local velocity versus time curves is often misleading and particularly during the initial phase of impact. It is therefore important to use a global variable such as axial momentum (Fig. 11), or kinetic energy which is not affected by wave effects and oscillations within the missile. Figure 11 shows that the axial momentum decreases approximately linearly with time and until the arrival of the tensile wave from the back face induces a change in the phenomenological process.

For projectile impacts having the physical and impulse characteristics of the types considered in this study, it is seldom required that the overall target response be simulated.

For hard projectiles impinging on a concrete slab, much computational economy can be gained by using a reduced lateral dimension. However, great care must be taken to prevent reflected waves in the slab plane from interfering with the calculations when the simulation time approaches the following value :

$$t = (L - D)/ 2C_{\ell} \qquad (20)$$

where L is the shortest in-plane slab dimension and C_{ℓ} is the longitudinal wave speed in concrete ($\simeq$ 0.45 cm/μ sec).

An interesting design aspect is that an increase in slab thickness will prolong the shock phase and consequently increase the initial kinetic energy loss. For the case at hand, the axial momentum is decreased to 70% of its initial value and the kinetic energy to about 40%. Doubling the thickness to 100 cm would result in the axial momentum decreasing to 45% and the kinetic energy to about 20%.

The penetration provides a decrease of momentum of about 5%.

The simulated missile penetration during the shock phase is about 3 cm (225 μsec), which agrees well with experimental data.

We have not simulated oblique impacts because they did not constitute an axisymmetrical type of problem. Effectively, for an oblique penetration, the plane wave generated by the projectile is reflected as a tensile wave, at an angle, away from the projectile axis and thus partly preserving the concrete ahead of the missile.

6. Design Considerations

Our study efforts and results suggest a relatively integrated and straightforward approach to the safety evaluation or design of concrete structures which may be subjected to hard projectile impacts.

During the shock phase, the pressure generated ahead of the missile, is a function of velocity and of concrete properties and is independent of the missile's mass M or of its diameter D. The rate of momentum decrease $\dot{R}$ represented by the slope of the initial straight line as shown in Figure 11, can be obtained from a single relatively short computer simulation. Given an initial velocity V_o and missile diameter D_o, as used in the single computer simulation, and resulting in a calculated value for $\dot{R}_o$, it then becomes possible to extrapolate to other projectile sizes but having the same velocity V_o as follows :

$$\dot{R}_i = \dot{R}_o \left(\frac{D_i}{D_o}\right)^2 \qquad (21)$$

where the subscript i refers to a projectile of mass M_i and of diameter D_i.

We define the shock phase duration time t_s, as

$$t_s = e/C_{\ell} \qquad (22)$$

where e is the concrete wall thickness.

The residual kinetic energy of the projectile at the end of the shock phase or at the onset of the penetration phase is expressed as follows :

$$E_s = \frac{1}{2} M_i \left| V_o + \frac{\dot{R}_o}{M_i} \left(\frac{D_i}{D_o}\right)^2 t_s \right|^2 \qquad (23)$$

Since R_o is a function of V_o and material properties, parametric studies are presently being performed to obtain a convenient semi-empirical formulation between $\dot{R}_o$ and V_o.

The residual kinetic energy must then be absorbed in the subsequent penetration and grid-stretching phases.

The penetration phase will decrease the momentum of the projectile by an amount ΔR_o equal to no more than 10% of the initial value. The amount of energy thus absorbed is estimated as

$$E_p = \frac{1}{2M_1} \Delta R_o \qquad (24)$$

The penetration phase is presently being studied in greater detail.

We then estimate the kinetic energy absorbed by the wall during the grid stretching phase.

The projectile is now ready to hit the rebars with a known amount of residual energy. Furthermore, at this point, the rebars are free of concrete within an area of diameter D_c. This diameter represents the back face crater diameter and is easily evaluated using eq. 19.

We can estimate the amount of energy absorbed by stretching to rupture the circular reinforcement net thus formed. We assume that the steel rebars contained within the back face crater diameter and intersected by the projectile face are stretched to their ultimate tensile strain.

The upper bound for energy absorbtion can then be evaluated as follows :

$$E_n = s_e \times V \qquad (25)$$

where s_e represents the strain energy density at rupture while V represents the volume of steel which is assumed stretched to rupture at the crater boundary. Stress concentrations during stretching would undoubtebly reduce the energy absorbing capacity of the rabar net.

The residual energy of the projectile after perforation, as it leaves the back face, is then

$$E_{res} = E_o - (E_s + E_p + E_n) \qquad (26)$$

The projectile may, of course, stop in the wall if its initial kinetic energy E_o is completely dissipated before perforation. Both theory and experimental evidence show, however, that even if complete perforation was not achieved, loss of airtightness may still result in the vicinity of the impact area.

7. Conclusions

Key phenomenological aspects of the physical processes involved in a hard missile impact on a reinforced concrete structure are now mostly understood, and have been properly modeled and simulated when compared to experimental results obtained from the US, France, Germany, the UK and Australia. In this paper, we have used, for presentation purposes, data obtained from Electricité de France's experimental program.

We have been able to identify and to define three distinct phases when a hard missile penetrates a reinforced concrete structure; these are the SHOCK, PENETRATION and GRID DEFORMATION phases.

Evaluating the effects of the shock phase requires detailed simulation and the use of a complex and advanced computer code package of the PISCES 2DELK type; furthermore, because of time considerations, the only effective target mass or volume of influence to be considered in simulating is that represented by the slab thickness and a front face circular area having its centre at the point of impact and a radius about 2.5 times the thickness of the slab.

The effects of the penetration phase are easily predictable and require simple computer programs for proper evaluation and, for most cases, only the use of proper tables and graphs.

The effects of the grid deformation phase are expected to be straight forward, require no special tools or techniques, and fall within the state of the art of everyday engineering.

The tools, techniques and concepts employed herein have required minimal assumptions, and form what may be called a multidisciplinary, integrated approach. With proper care in analysis, we believe much additional insight can be gained through application of this approach to the prediction of structural behavior under the loading conditions identified, defined and evaluated in this study.

References

|1| KENNEDY, R.P., "A Review of Procedures for the Analysis and Design of Concrete Structures to Resist Missile Impact Effects", ELCALAP International Seminar, Berlin, 8-19 September, 1975, Paper 51/1.

|2| GODBOUT, P.J., BRAIS, A., "A Methodology for Assessing Aircraft Crash Probabilities and Severity as Related to the Safety Evaluation of Nuclear Power Stations - Phase II", Report to the Atomic Energy Control Board of Canada, September, 1976.

|3| FIQUET, G., DACQUET, S., "Study of the Perforation of Reinforced Concrete Slabs by Rigid Missiles - Experimental Study, Part II", Nuclear Engineering and Design, Vol. 41, pp. 103-120, 1977.

|4| "Dynamics of a Blunt Projectile Impacting on Concrete at 1,400 fps", Physics International Company, San Leandro, Cal., PIFR-663, 1975.

|5| ATTALLA, I., NOWOTNY, B., "Missile Impact on a Reinforced Concrete Structure", Nuclear Engineering and Design, Vol. 37, pp. 321-332, 1976.

|6| HANCOCK, S.L., "PISCES-2DELK, Finite Difference Equations", Physics International Company, San Leandro, Cal., Technical Memo TCAM 76-2, April, 1976.

|7| GREEN, S.J., SWANSON, S.R., Terra-Tek Inc., Salt Lake City, Utah, Technical Report No. AFWL-TR-72-2, April, 1973.

|8| BERRIAUD, C., and al., "Local Behavior of Reinforced Concrete Walls Under Missile Impact", Nuclear Engineering and Design, Vol. 45, pp. 457-469, 1978.

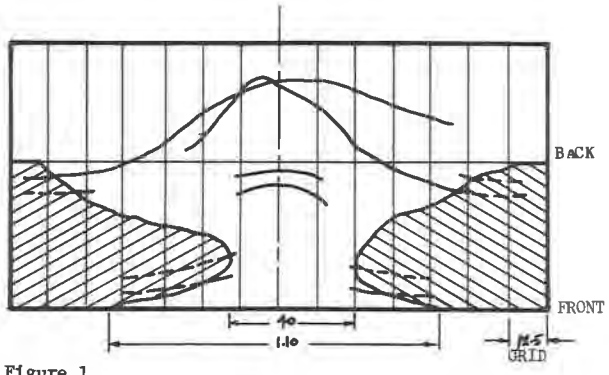

Figure 1.

Vertical section after impact with loose concrete removed (from ref. 3.).

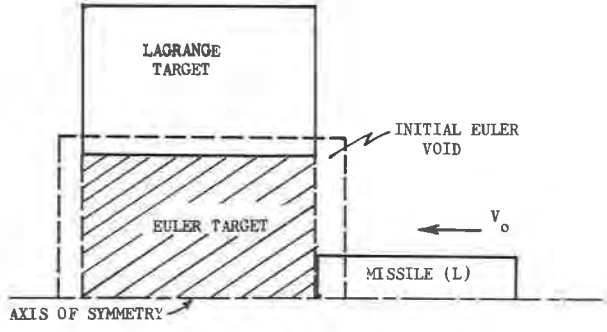

Figure 2.

Axisymmetrical grid set up for PISCES 2DELK impact simulation.

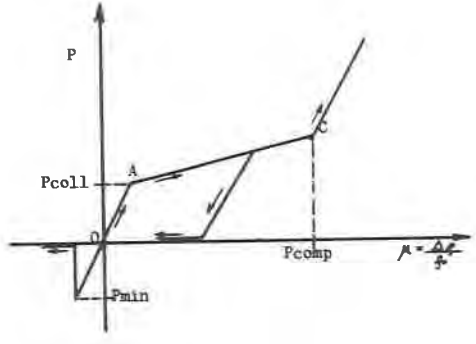

Figure 3.

Basic equation-of-state model for concrete at low impact velocities.

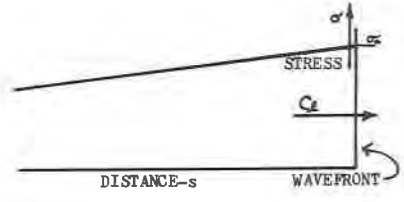

Figure 4.

Assumed shape of stress pulse following impact.

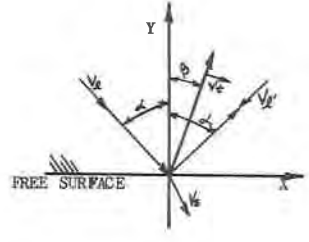

Figure 5.

Wave reflections and particule motion associated with oblique incidence.

A : Incident dilatational wave

B : Reflected dilatational wave

C : Generated shear wave

D : Surface motion

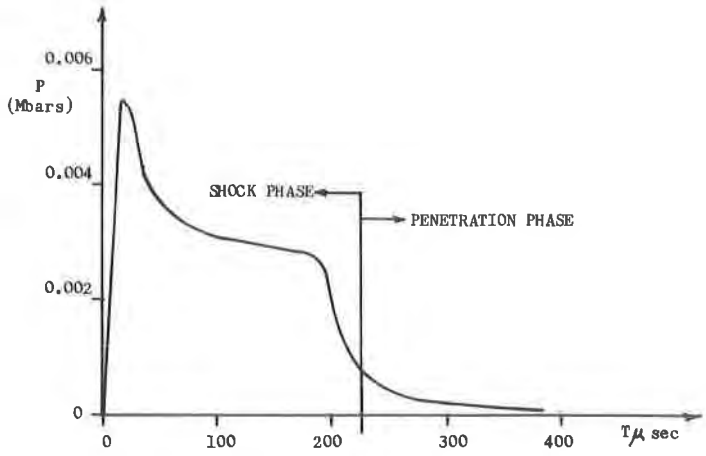

Figure 9. Typical plot of average pressure at Projectile-Target interface as a function of time.

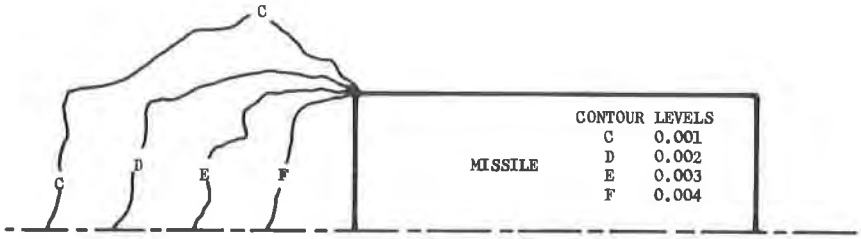

Figure 10. Pressure contours ahead of projectile during shock phase (Units = M bars).

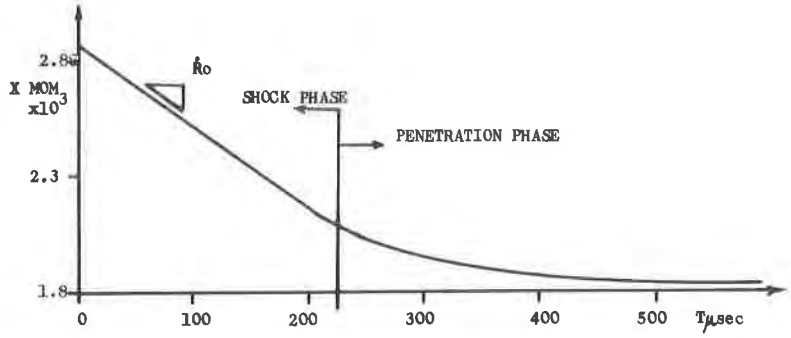

Figure 11. Typical plot of projectile axial momentum as a function of time (Units = gr·cm/μsec).

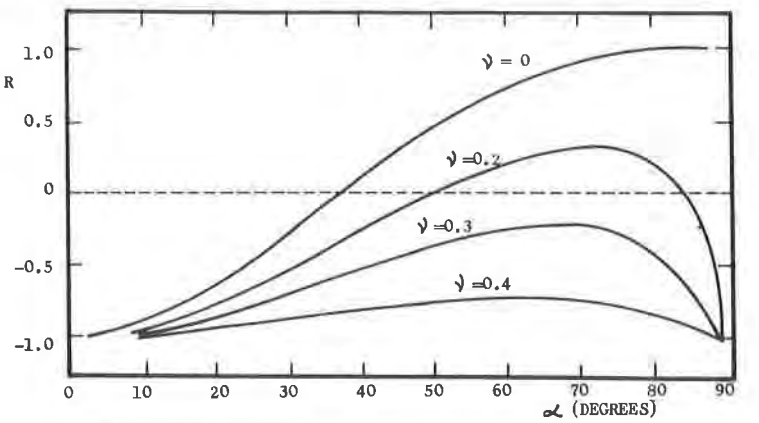

Figure 6. Coefficient of reflection R as a function of the angle of incidence α for several values of Poisson's Ratio ν (ν concrete is about 0.19).

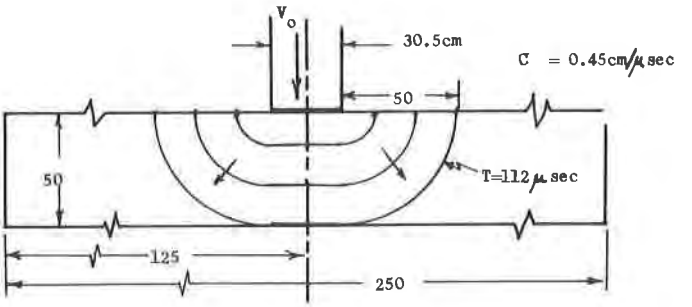

Figure 7. Stress wave front propagation for the experimental set up previously described.

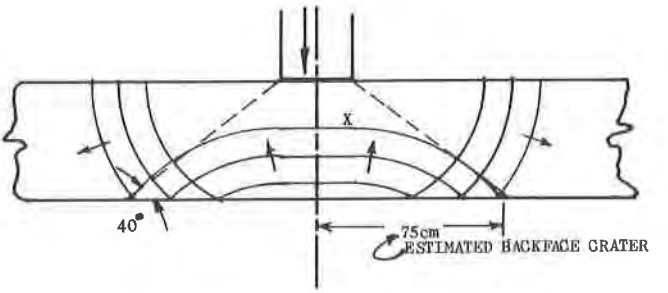

Figure 8. Stress wave front propagation and reflection. Concrete between the back face and curve "x" is fractured (see Figure 1.).